

## Solidification behavior and Laves phase dissolution during homogenization heat treatment of Inconel 718 superalloy

Mohammad Javad Sohrabi, Hamed Mirzadeh\*, Mohsen Rafiei

*School of Metallurgy and Materials Engineering, College of Engineering, University of Tehran, P.O. Box 11155-4563, Tehran, Iran*

### ARTICLE INFO

**Keywords:**  
Nickel-based superalloys  
Solidification  
Microstructure  
Segregation  
Homogenization

### ABSTRACT

The solidification behavior and microstructural evolutions during homogenization heat treatment of Inconel 718 superalloy were studied. The microstructure of the as-cast alloy was characterized by optical micrographs, scanning electron microscopy (SEM) images, and elemental analysis based on energy dispersive spectroscopy (EDS). The optimum etching techniques, especially electroetching, were characterized to reveal the dendritic nickel matrix, the microsegregation between dendrite arms, and the austenite/Laves eutectic structure. The elemental analysis of different microstructural features, especially the variation of the chemical composition of austenite, was successfully related to the pseudo-binary solidification constitution diagram. Moreover, the extension of the nonequilibrium eutectic isotherm was evaluated to unravel the solidification path of this important engineering alloy. The dissolution of the Laves phase and its kinetics during exposure at elevated temperatures with the purpose of homogenization were also discussed.

### 1. Introduction

Nickel-based superalloys are austenitic precipitation hardening alloys, which are important structural materials for many engineering applications [1–6]. Among them, Inconel 718 is more popular than any other superalloy. This alloy is precipitation strengthened by special alloying elements such as Nb and also contains refractory elements such as Mo [7–10]. The presence of these elements makes the alloy susceptible to severe microsegregation between dendrite arms and formation of undesirable Laves phase. The latter is considered as a type of harmful topologically close-packed (TCP) phases. On the one hand, the heavily solute concentration regions are highly detrimental to fatigue life. On the other hand, the Laves phase is associated with decreased mechanical performance due to consumption of a large amount of Nb as the principal element required for precipitation hardening of the alloy. Its own brittle nature and low melting point [11–13] are also problematic. The likelihood of its presence increases as the solute segregation of the ingot increases.

The solidification of Alloy 718 and other Nb-bearing austenitic superalloys begins with the formation of Nb-lean austenitic dendrites. Interdendritic eutectic-type solidification constituents involving MC-type carbides and a Nb-rich Laves phase occur in these alloys. While it has been stated that the austenite/Laves eutectic constituent terminates solidification in these alloys [14], it is not clear how the eutectic reaction takes place in alloys with Nb content lower than the eutectic start

point at 9.6 wt%. Niobium is the dominant element in the evolution of solidification microstructure with C and Si affecting the amounts of austenite/MC and austenite/Laves constituent observed. In Alloy 718 with high amount of Nb (4.75–5.5 wt%), austenite/Laves eutectic is the predominant minor constituent observed beside the austenite phase [14].

During reheating, there is an incipient melting temperature (IMT) associated with the presence of undesirable phases, which is reported to be between 1160 and 1180 °C [15–17]. The dissolution of Laves phase occurs during exposure at elevated temperatures (but lower than IMT) by back-diffusion of the solute atoms from the solute-rich regions into the matrix without local melting [15]. This homogenization treatment plays an essential role in obtaining uniform microstructures free from harmful phases [10,15–20]. The exposure temperature is considered close to the IMT to decrease the required homogenization time.

While the solidification behavior of Inconel 718 has been studied so far [21–24], the interpretation of the presence of obtained phases and their chemical composition based on the phase diagram has not been unraveled completely. In fact, it is not clear how the eutectic reaction takes place in the Inconel 718 alloy with Nb content of ~5 wt%, which is lower than the eutectic start point at 9.6 wt% Nb. Thus, this subject needs more experimental work by consideration of rigorous elemental and microstructural analyses to unravel the solidification path of this alloy. Moreover, the etching techniques for studying the as-cast structure of Inconel 718 for characterization of microstructural features

\* Corresponding author.

E-mail address: [hmirzadeh@ut.ac.ir](mailto:hmirzadeh@ut.ac.ir) (H. Mirzadeh).

**Table 1**  
Chemical composition (wt%) of the as-cast Inconel 718 superalloy.

Fe	Cr	Nb	Mo	Ti	Al	C	Ni
18.88	17.61	4.97	2.85	0.94	0.57	0.022	Balance

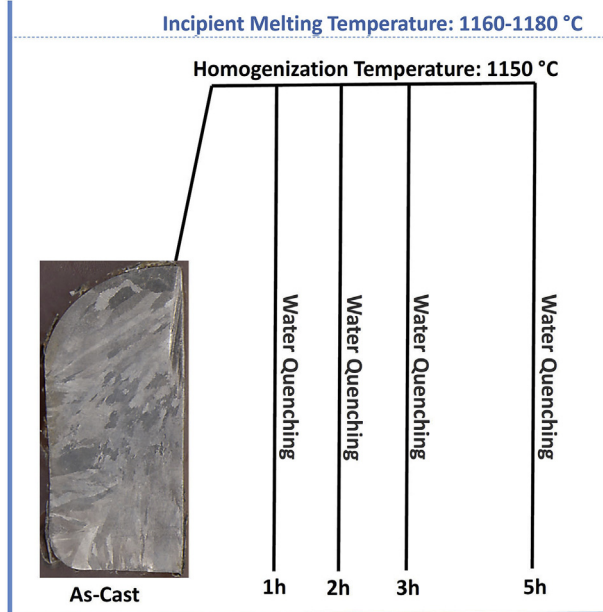
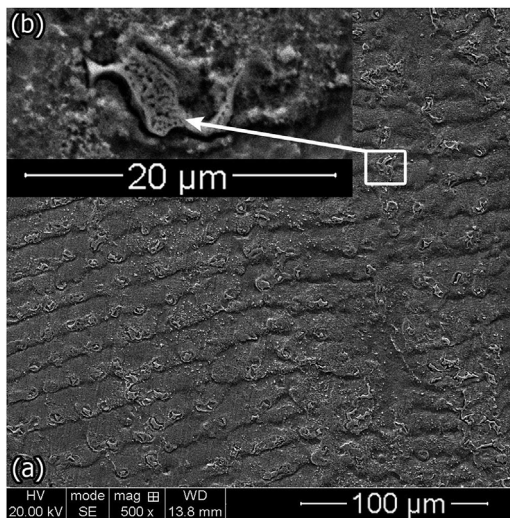


**Fig. 1.** Schematic representation of the heat treatment routes along with the macrostructure of the as-cast ingot revealed by Kalling's reagent number 2.

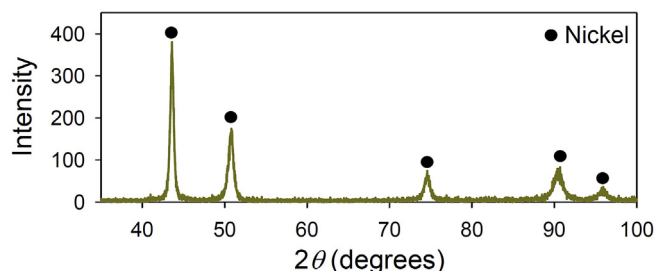
(austenite dendrites, segregated regions, and eutectic structure) based on more appropriate chemical and electroetching techniques need to be reevaluated and compared with the usual procedure. Therefore, the present work aims to deal with the solidification behavior of Inconel 718 superalloy and metallographic etching. Afterward, the homogenization treatment for dissolution of Laves phase will be discussed.

## 2. Experimental details

A forged Inconel 718 superalloy was vacuum arc remelted and cast in a water-cooled copper mold (with dimensions of  $6 \times 2.5 \times 1 \text{ cm}^3$ ) to



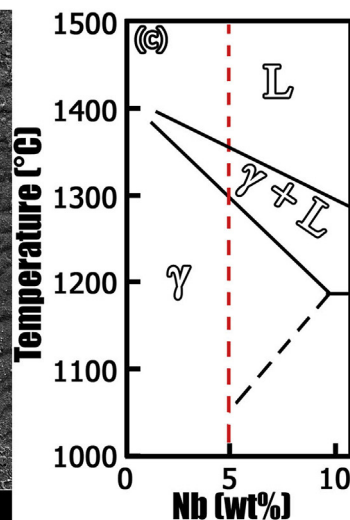
**Fig. 2.** (A) and (B) SEM images of the as-cast ingot revealed by Kalling's reagent number 2 and (C) Part of the representative pseudo-binary solidification constitution diagram [14].



**Fig. 3.** XRD patterns taken from the as-cast alloy.

obtain a superalloy with chemical composition as shown in Table 1. It can be seen that the Nb content of the as-cast alloy is close to the nominal composition reported for Inconel 718 alloy (5 wt%) [13]. The homogenization treatment was performed at 1150 °C for holding durations of 1, 2, 3, and 5 h as schematically shown in Fig. 1. The choice of this temperature was based on the reported range of IMT (1160–1180 °C [15–17]) and the idea that the homogenization temperature should be as high as possible. It should be noted that Miao et al. [16] and Liang et al. [17] have considered homogenization temperatures of 1140 and 1160 °C, respectively. Therefore, the heat treatment route is consistent with the usual procedure. A muffle furnace having the temperature control system with the accuracy of  $\pm 3$  °C was used for these thermal treatments.

Samples were grinded and polished using standard sample preparation techniques for metallographic observations. The microstructural features were revealed by Kalling's reagent number 2 (100 ml HCl – 100 ml ethanol – 5 g CuCl<sub>2</sub>) as the standard chemical etchant for nickel-based superalloys [25,26]. A Vega Tescan scanning electron microscope (SEM) was used for microstructural studies. The SEM was equipped with the Bruker QUANTAX XFlash 6 detector for energy-dispersive spectroscopy (EDS) and it was used for elemental analysis, which integrates a true standardless P/B ZAF correction technology. These corrections are based on the fact that the intensity of the emitted characteristic X-rays is influenced by the atomic-number effect (Z), the absorption effect (A), and the fluorescence excitation effect (F). Finally, phase identification was performed by X-ray diffraction (XRD) technique using a PHILIPS diffractometer with Cu- $\kappa\alpha$  radiation, where the  $2\theta$  angles between 30 and 100°, a step size of 0.02°, and a scan rate of 3°/min were used.



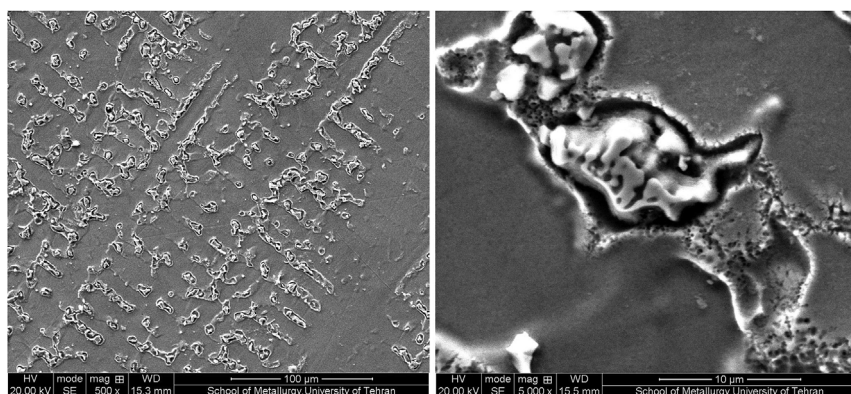


Fig. 4. SEM images of the as-cast ingot revealed by a sulfuric acid solution.

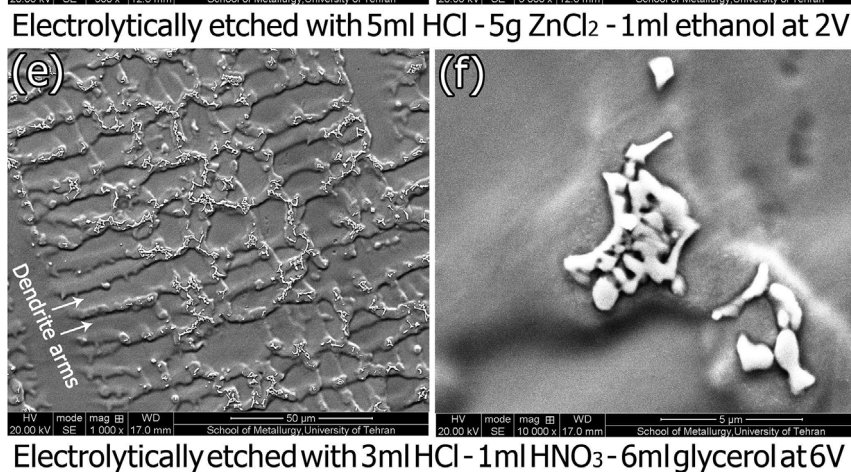
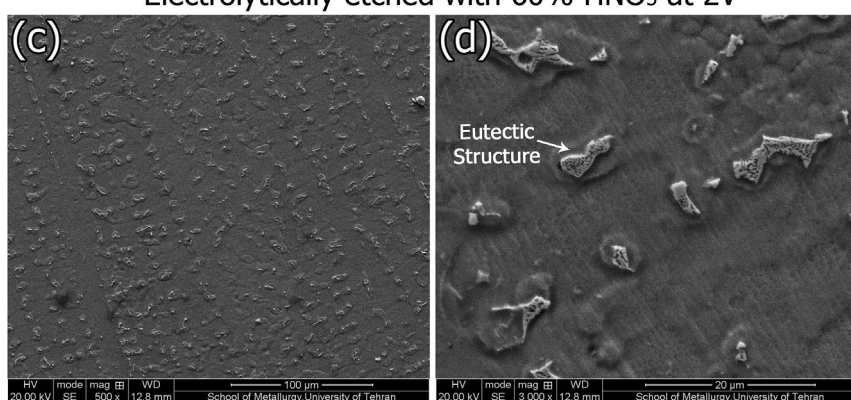
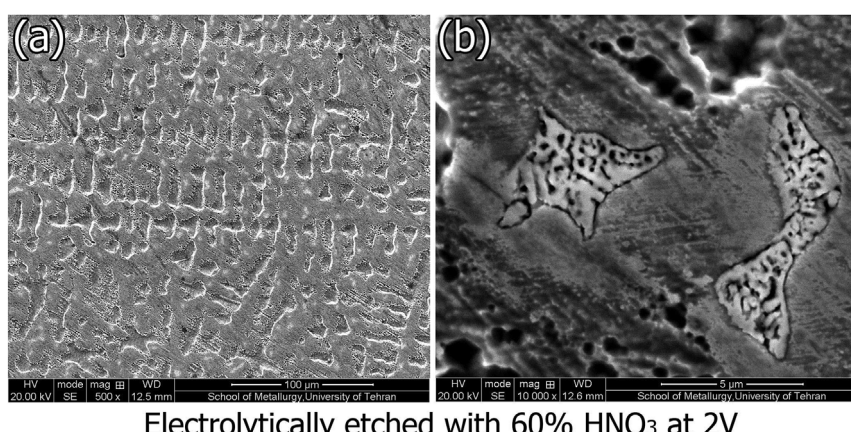
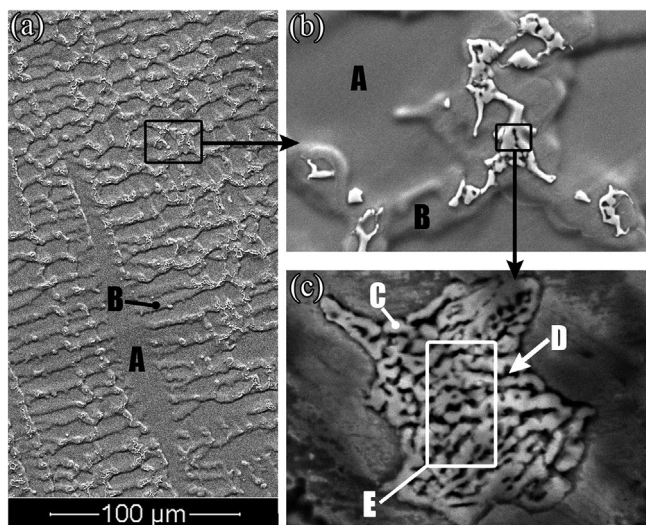


Fig. 5. SEM images of the as-cast ingot revealed by various etchants.



**Fig. 6.** SEM images of the as-cast microstructure with identification of different microstructural constituents.

### 3. Results and discussion

#### 3.1. As-cast microstructure

SEM images of the as-cast alloy along with part of the representative pseudo-binary solidification constitution diagram are shown in Fig. 2. It can be seen in Fig. 2a that the as-cast alloy is mainly consisted of austenite dendrites as well as some eutectic structures between dendrite arms. A SEM image at higher magnification is shown in Fig. 2b, where the presence of the eutectic constituent is evident. The phase diagram shown in Fig. 2c implies that the eutectic structure should not be present for a composition with ~5 wt% Nb. This eutectic structure has been characterized as austenite/Laves eutectic in previous works [14] but its formation needs to be unraveled. This will be considered in Section 3.4. Meanwhile, the XRD patterns taken from the as-cast alloy are shown in Fig. 3, where it can be seen that only austenite peaks can be identified. This might be related to the limitations of the XRD technique for revealing phases with low volume fractions. However, Fig. 2 provides evidences for the presence of another phase, undoubtedly. However, it seems that Kalling's reagent number 2 is not an optimum etchant for this purpose and it is required to study the metallographic etching more rigorously as will be treated in Section 3.2.

#### 3.2. Metallographic etching

The as-cast microstructure was etched with another common etching technique: electroetching using a sulfuric acid solution [25] as shown in Fig. 4. It can be seen that electroetching can better reveal the presence of the eutectic constituent present in the interdendritic areas. However, the segregated regions, themselves, were not revealed clearly. This implies that for studying the solidification behavior, more appropriate etching techniques are required. Therefore, several etchants based on different references [16,25–29] were evaluated and modified and the final results are shown in Fig. 5.

Fig. 5a and b demonstrate that the  $\text{HNO}_3$  solution can reveal dendrite arms and eutectic structure, perfectly. It has been shown by Mirzadeh and coworkers [27,28] that electroetching with  $\text{HNO}_3$  solution is one of the most appropriate etching techniques for austenitic stainless steels and it can be seen that the same idea works for the austenitic superalloys. Fig. 5c and d shows the results of the electroetching with a modified version of the Lucas reagent [29], which only shows the eutectic constituent. Fig. 5e and f depict the most appropriate technique, which can reveal the dendrite arms, segregated regions, and

the Laves phase. This etching solution is a modified version of the etchant used by Miao et al. [16]. Therefore, this technique was used in the present work.

#### 3.3. Elemental analysis

The as-cast microstructure at different magnifications is shown in Fig. 6, where different letters (A to E) have been assigned to different regions: "A" represents the dendrite core, "B" denotes the interdendritic region, "C" depicts the Laves phase, "D" represents the interlamellar austenite (pertaining to the austenite/Laves eutectic), and "E" denotes the eutectic structure.

EDS point analyses taken from these areas are shown in Fig. 7. It can be seen that A, B, C, D, and E have 2.17, 4.48, 24.05, 7.90, and 20.61 wt % Nb, respectively. It can be surmised that the dendrite core (Point A) is a Nb-lean region. However, the interdendritic region (Point B) is much more enriched with Nb due to microsegregation. The niobium content of the Laves phase (Point C) is ~24 wt% that is consistent with the range of 22.3–26 wt% reported in previous research works [11,14,21,30,31] and its Mo content is higher than the Mo content of the alloy. The interlamellar austenite (Point D) exhibits 7.90 wt% Nb, which is relatively consistent with the value of 9.6 wt% [21] or 9.3 wt% [31], where this small difference can be ascribed to the limitations of the EDS technique for point analysis. Finally, the eutectic structure (Point E) exhibits 20.61 wt% Nb, which is comparable with the reported value of 19.1 wt% [14].

Fig. 8 represents the EDS maps taken from a region containing the Laves phase. It can be seen that the Laves phase is Nb- and Mo-rich but its Ni, Cr, and Fe contents are lower than austenite. The atomic percents of the elements in the Laves phase are shown in Table 2. It has been reported that the Laves phase is an intermetallic compound represented as  $(\text{Ni},\text{Fe},\text{Cr})_x (\text{Nb},\text{Mo},\text{Ti})$  or  $\text{Ni}_y\text{Nb}$ , where  $x$  is generally regarded to be 2 and  $y$  has been reported in every research as 2 [11,14,15]. However, by consideration of weight percents reported in previous works and conversion to atomic percents,  $x$  can be determined as 2.69 [11], 3.97 [14], and 3.37 [31] and  $y$  can be determined as 2.1 [11], 3.25 [14], and 2.71 [31]. Based on Tables 2,  $x$  and  $y$  can be determined as 2.92 and 2.06, respectively. According to these works and the present study, it can be deduced that  $x$  and  $y$  of respectively 3 and 2 are reasonable.

#### 3.4. Solidification behavior

The solidification of superalloys can be followed from the phase diagram. However, the kinetics of the solidification process determines the microstructure that actually is formed [13]. In fact, solvent-lean phase forms first and then grows, usually by dendritic solidification, in the directions of heat and alloy gradients. What makes the solidification of superalloys outstandingly different from less sophisticated alloys is that the solute contents of these alloys are very high [13]. The phase diagram is shown in Fig. 9, where O-D-E-C represent the equilibrium diagram but this equilibrium diagram cannot justify the presence of the eutectic structure as demonstrated in previous section. A nonequilibrium phase diagram has been provided by Donachie and Donachie [13], where a nonequilibrium eutectic isotherm is roughly extended from 9.6 (Point D) to ~4 wt% Nb.

It is supposed that this extension is highly sensitive to the chemical composition and solidification conditions, which can be represented by the amount of eutectic structure. Therefore, the key point to unravel the solidification behavior is behind this nonequilibrium point, which is shown by Point B in Fig. 9. Therefore, it was assumed that the composition of Point B should be in accordance with the amount of eutectic constituent (based on the simple lever rule). For this purpose, beside SEM images, optical micrographs at low magnifications were also used to estimate the volume fraction of the eutectic structure, which was determined as 4.8%. Based on the results reported by Ling et al. [32], the density of austenite and Laves phases are not very different.

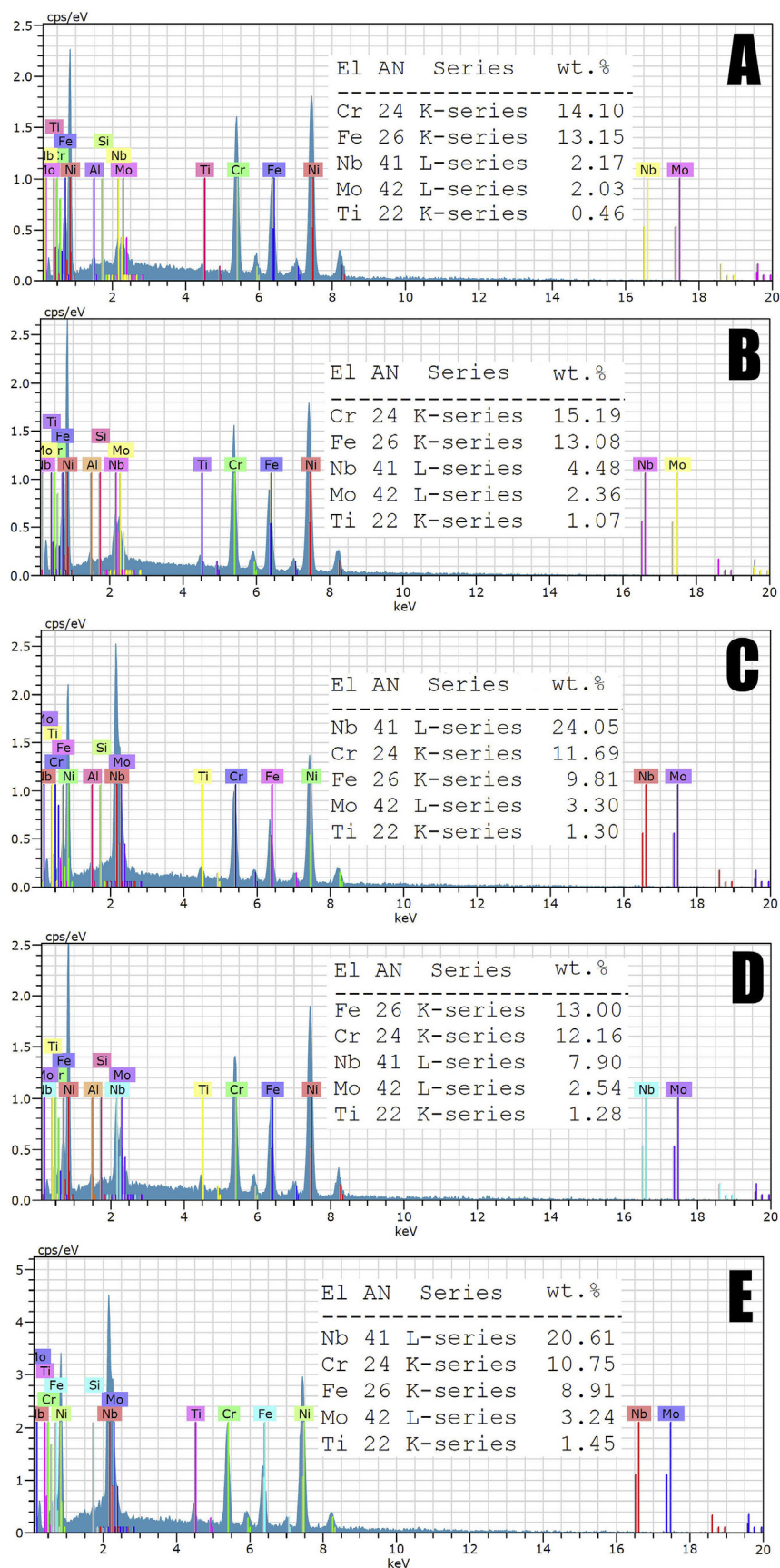
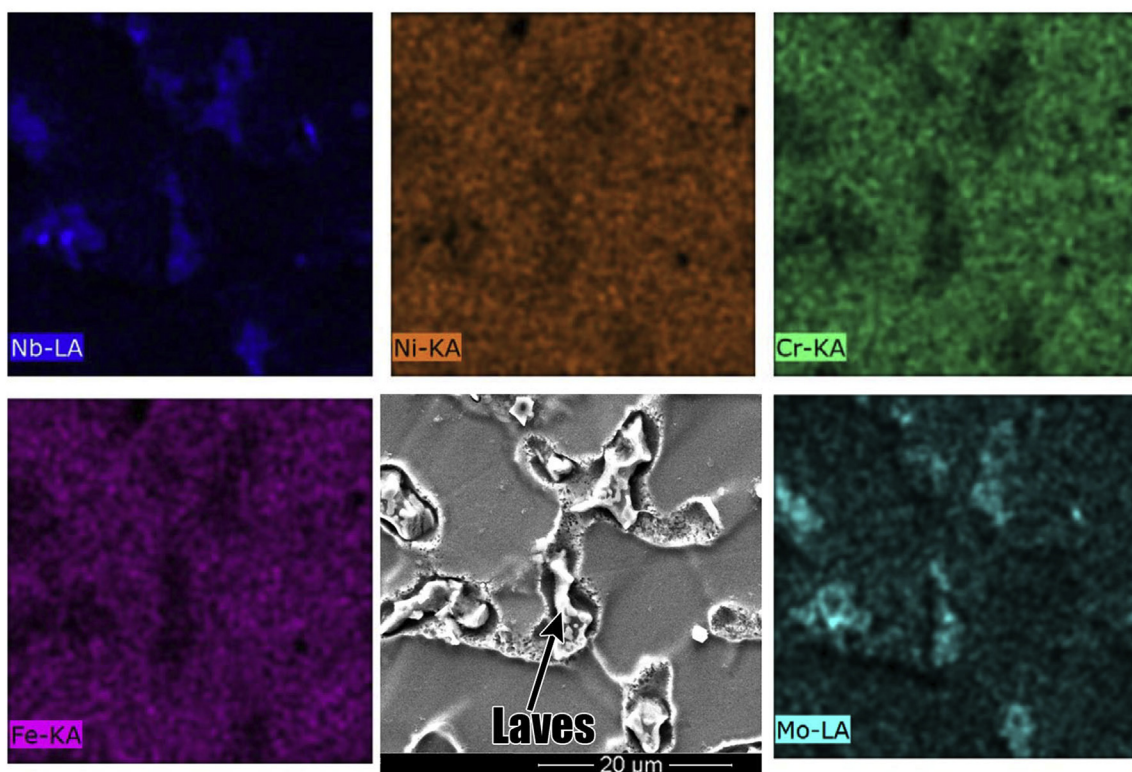


Fig. 7. EDS point analysis of different microstructural constituents shown in Fig. 6.



**Fig. 8.** EDS maps taken from a region containing the Laves phase.

**Table 2**

Atomic percents of the elements in the Laves phase as determined by EDS point analysis.

Ni	Fe	Cr	Nb	Mo	Ti
42.57	13.99	17.91	20.62	2.74	2.16

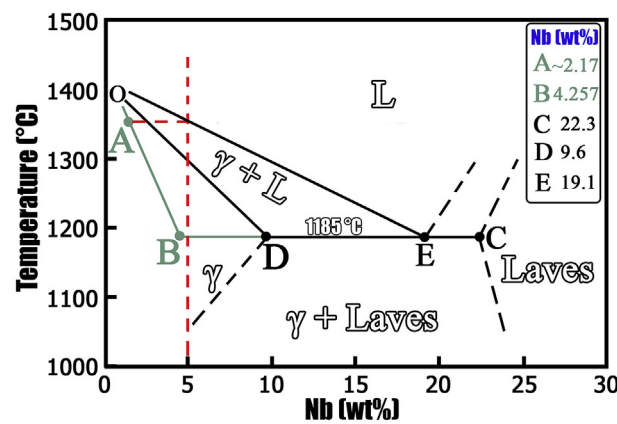


**Fig. 9.** Pseudo-binary solidification constitution diagram (as represented by O-D-E-C) [14] and the extension of the nonequilibrium eutectic isotherm (as represented by B-D).

Therefore, the value of 4.8% was considered as the weight percent of the eutectic structure (Point B). Now, based on the lever rule,  $(4.97 - Nb_B)/(19.1 - Nb_B) = 0.048$ , and hence,  $Nb_B$  can be determined as 4.257 wt%, which is consistent with the rough estimate of ~4 wt% [13,31].

Now, based on Figs. 7 and 9, it is possible to follow the solidification sequences. Note that the indicated points (A to E) in Fig. 7 are in accordance with those shown in Fig. 9. The first solidified austenite

should have a composition shown by Point A, where the equilibrium Nb is around 3 wt% [13] and it will decline by consideration of the nonequilibrium line (O-B), which was determined by EDS as 2.17 wt% in Fig. 7. Afterward, Nb will be rejected from the solidifying dendrites, where it will reach the 4.257 wt% in the interdendritic areas based on point B shown in Fig. 9. This value is consistent with that determined by EDS as 4.48 wt% in Fig. 7. Now, small amount of liquid will remain (4.8 wt%), which will reach the eutectic composition of 19.1 wt% (Point E) in Fig. 9. This value is close to the value of 20.61 wt% determined by EDS in Fig. 7. Finally, this remaining liquid will eutectically react to produce austenite/Laves eutectic structure. The Laves phase should have 22.3 wt% Nb based on Point C in Fig. 9, where it was determined as 24.05 wt% Nb by EDS in Fig. 7. The Nb content of the interlamellar austenite might be determined from Points B or D in Fig. 9. However, it is widely known that the eutectic structure has a fixed composition for its constituents. Therefore, it is expected that Point D with 9.6 wt% Nb in Fig. 9 represents the Nb content of the interlamellar austenite. The Nb content of the interlamellar austenite was determined as 7.90 wt% Nb by EDS in Fig. 7. This value is relatively consistent with the value of 9.6 wt% Nb for Point D in Fig. 9. As a result, it can be deduced that the solidification of the alloy 718 in this work follows the aforementioned sequences.

### 3.5. Homogenization

The effect of homogenization at 1150 °C on the microstructure is shown in Fig. 10. It can be seen that the Nb-rich segregated areas tend to disappear and the volume fraction of the Laves phase decreases by increasing homogenization time. The former can be ascribed to the diffusion of segregated elements and decreasing contrast between dendrite arms and segregated regions. The latter can be attributed to the back-diffusion of the atoms from the Laves phase into the matrix. The dependence of the volume fraction of the Laves phase on the homogenization time is shown in Fig. 11, where a mathematical formula has been fitted on the data (as shown in the figure). The required

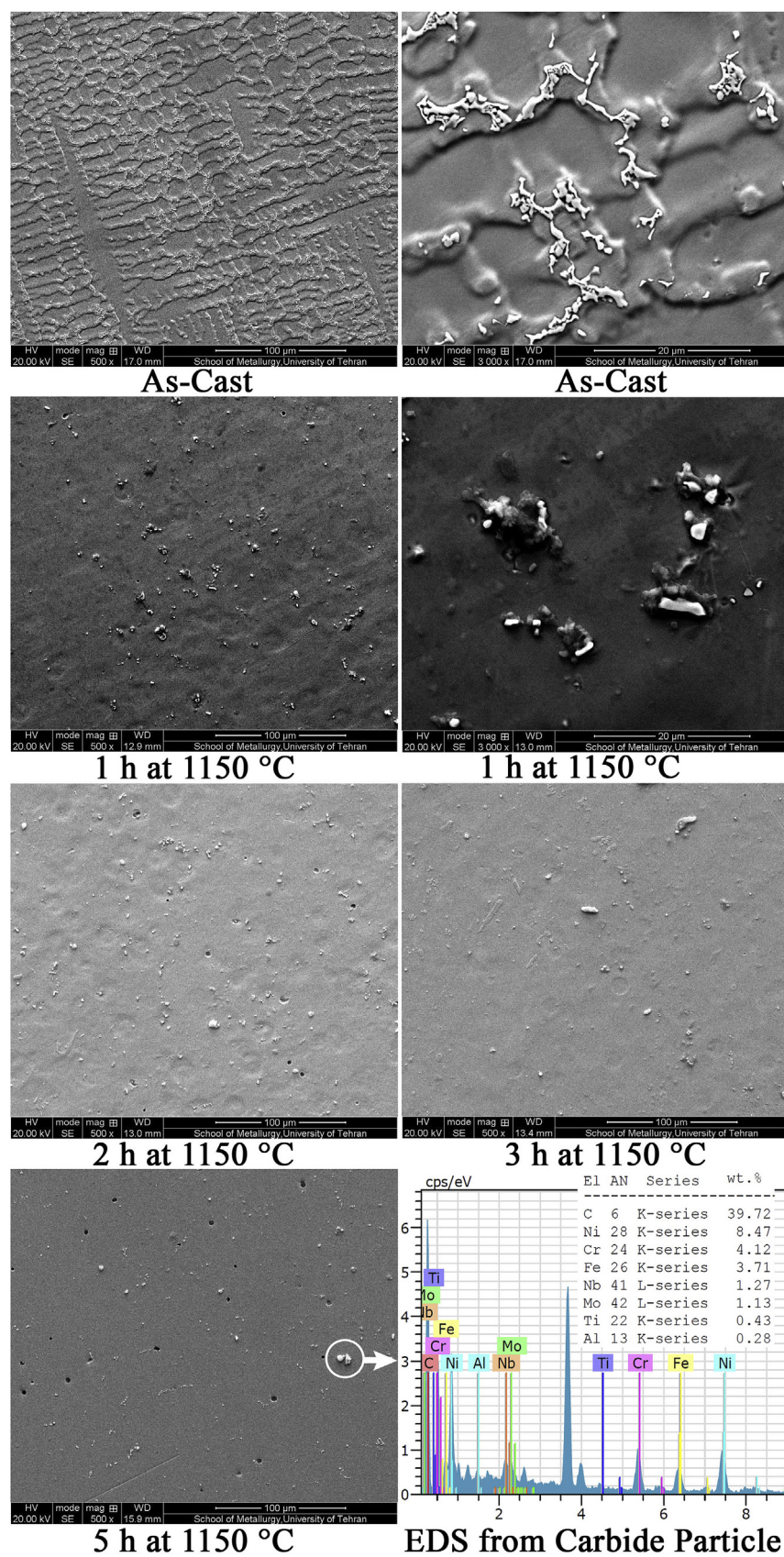


**Fig. 10.** Microstructural evolution during homogenization treatment at 1150 °C along with the EDS map taken from the carbide particles.

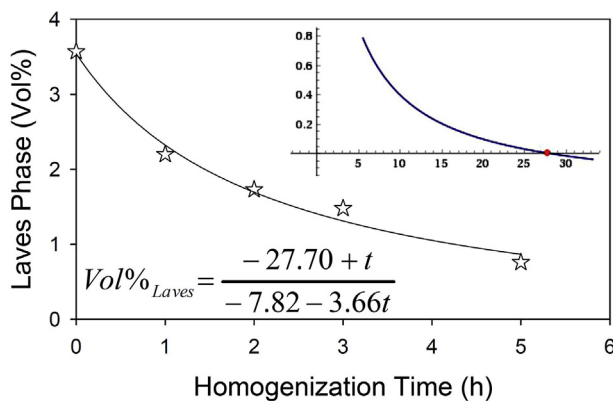


Fig. 11. The dependence of the volume percent of the Laves phase on homogenization time at 1150 °C.

time for the dissolution of the Laves phase can be estimated by this formula as 27.7 h. It should be noted that the required time at homogenization temperatures of 1140 °C [19] and 1160 °C [17] was determined as 35 and 13 h, respectively. Therefore, the estimated value in the present work is reasonable. The required time for the elimination of Laves phase ( $t_{\text{Laves}}$ ) has been estimated by  $t_{\text{Laves}} = A \exp(-0.036T)$  [17], where  $A$  represents the segregation degree of the ingot and  $T$  is the homogenization temperature in degree Celsius. The parameter  $A$  was determined as  $2.64 \times 10^{19}$  in the present work. This parameter has been determined as  $2.33 \times 10^{19}$  by Miao et al. [16], which is lower than the calculated value in the present work. Note that the amounts of the as-cast Laves phase in the present investigation and the work of Miao et al. [16] are respectively 3.57% and 3.2%, which is consistent with more severe segregation degree in the present work (higher  $A$  value). Note that, in general, the amount of the Laves phase is dependent on the Nb content and cooling rate [33].

Fig. 10 also reveals that the microstructure of the 718 alloy in the present work also contains carbide particle, consistent with previous works [14,16,17]. As shown in Fig. 10, for the homogenization time of 5 h, small amount of the Laves phase still exists but the presence of the carbide particles is evident. The latter was also supported by the EDS point analysis as shown in Fig. 10. In fact, the formation of carbide particles occurs at temperatures much higher than 1150 °C [14,30]. This carbide particles present in the as-cast condition, but like the Laves phase, these carbides are white-etching matters and their detection in the as-cast condition is difficult. However, during homogenization, by the dissolution of the Laves phase, these carbides became discernible.

#### 4. Conclusions

The solidification behavior and the dissolution of the Laves phase during homogenization of Inconel 718 superalloy were studied. The following conclusions can be drawn from this work:

- (1) Chemical etching by the renowned Kalling's reagent number 2 was found to be not the most appropriate technique to clearly distinguish the dendritic nickel matrix, the microsegregation between dendrite arms, and the austenite/Laves eutectic structure. Several other etchants were evaluated, and conclusively, electroetching by a solution containing 3 ml HCl – 1 ml HNO<sub>3</sub> – 6 ml glycerol at 6 V was selected as an optimum etching technique for microstructural analysis in the as-cast condition.
  - (2) The elemental analysis of different microstructural features, especially variation of the chemical composition of austenite, was successfully related to the pseudo-binary solidification constitution diagram. For this purpose, the extension of the nonequilibrium eutectic isotherm was taken into account and the estimations were based on the amount of the eutectic constituent (determined by
- image analysis) and application of the simple lever rule. Good correlation between the modified solidification constitution diagram and the experimental results were observed, which revealed that this approach is appropriate for unraveling the solidification path of Inconel 718 superalloy.
- (3) The dissolution of the Laves phase and its kinetics during exposure at 1150 °C with the purpose of homogenization were evaluated. It was revealed that the Nb-rich segregated areas tend to disappear and the volume fraction of the Laves phase decreases by increasing homogenization time. This happens by the back-diffusion of the solute atoms from the solute-rich regions into the matrix, where its driving force is the tendency to vanish these non-equilibrium segregated regions and phases. The required time for the dissolution of the Laves phase was estimated as ~28 h by mathematical fitting of the experimental data. During homogenization, by the dissolution of the Laves phase, the carbide particles became discernible, which were formed during solidification.

#### References

- [1] Y.C. Lin, H. Yang, L. Li, Effects of solutionizing cooling processing on  $\gamma''$  (Ni<sub>3</sub>Nb) phase and work hardening characteristics of a Ni-Fe-Cr-base superalloy, Vacuum 144 (2017) 86–93.
- [2] Y.C. Lin, F. Wu, Q.W. Wang, D.D. Chen, S.K. Singh, Microstructural evolution of a Ni-Fe-Cr-base superalloy during non-isothermal two-stage hot deformation, Vacuum 151 (2018) 283–293.
- [3] Y.C. Lin, F.Q. Nong, X.M. Chen, D.D. Chen, M.S. Chen, Microstructural evolution and constitutive models to predict hot deformation behaviors of a nickel-based superalloy, Vacuum 137 (2017) 104–114.
- [4] X.M. Chen, Y.C. Lin, X.H. Li, M.S. Chen, W.Q. Yuan, Investigation on strain dependence of metadynamic recrystallization behaviors of GH4169 superalloy, Vacuum 149 (2018) 1–11.
- [5] D.X. Wen, Y.C. Lin, Y. Zhou, A new dynamic recrystallization kinetics model for a Nb-containing Ni-Fe-Cr-base superalloy considering influences of initial  $\delta$  phase, Vacuum 141 (2017) 316–327.
- [6] X.M. Chen, Y.C. Lin, F. Wu, EBSD study of grain growth behavior and annealing twin evolution after full recrystallization in a nickel-based superalloy, J. Alloy. Comp. 724 (2017) 198–207.
- [7] K. Feng, P. Liu, H. Li, S. Sun, S. Xu, J. Li, Microstructure and phase transformation on the surface of Inconel 718 alloys fabricated by SLM under 1050 °C solid solution + double ageing, Vacuum 145 (2017) 112–115.
- [8] Q. You, S. Shi, X. You, Y. Tan, Y. Wang, J. Li, Evaporation behavior of Ni, Cr and Fe in Inconel 718 superalloy during electron beam smelting, Vacuum 135 (2017) 135–141.
- [9] L. Li, G. Peng, J. Wang, J. Gong, H. Li, Experimental study on weld formation of Inconel 718 with fiber laser welding under reduced ambient pressure, Vacuum 151 (2018) 140–147.
- [10] H. Qi, M. Azer, A. Ritter, Studies of standard heat treatment effects on microstructure and mechanical properties of laser net shape manufactured INCONEL 718, Metall. Mater. Trans. 40 (2009) 2410–2419.
- [11] J.J. Schirra, R.H. Caless, R.W. Hatala, E.A. Loria (Ed.), The Effect of Laves Phase on the Mechanical Properties of Wrought and Cast + HIP Inconel 718, Superalloys 718, 625 and Various Derivatives, The Minerals, Metals & Materials Society, 1991.
- [12] W. Sames, K. Unocic, R. Dehoff, T. Lolla, S. Babu, Thermal effects on microstructural heterogeneity of Inconel718 materials fabricated by electron beam melting, J. Mater. Res. 29 (2014) 1920–1930.
- [13] M. Donachie, S. Donachie, Superalloys a Technical Guide, second ed., ASM International, 2002.
- [14] M.J. Cieslak, G.A. Knorovsky, T.J. Headley, A.D. Romig, E.A. Loria (Ed.), The Solidification Metallurgy of Alloy 718 and Other Nb-containing Superalloys, Superalloy 718 Metallurgy and Applications, The Minerals, Metals & Materials Society, 1989.
- [15] E. Chlebus, K. Gruber, B. Kuźnicka, J. Kurzak, T. Kurzynowski, Effect of heat treatment on the microstructure and mechanical properties of Inconel 718 processed by selective laser melting, Mater. Sci. Eng. 639 (2015) 647–655.
- [16] Z.J. Miao, A.D. Shan, Y.B. Wu, J. Lu, W.L. Xu, H.W. Song, Quantitative analysis of homogenization treatment of INCONEL718 superalloy, Trans. Nonferrous Metals Soc. China 21 (2011) 1009–1017.
- [17] X. Liang, R. Zhang, Y. Yang, Y. Han, E.A. Loria (Ed.), An Investigation of the Homogenization and Deformation of alloy 718 Ingots, Superalloys 718, 625, 706 and Various Derivatives, The Minerals, Metals & Materials Society, 1994.
- [18] P.J. DiConza, R.R. Biederman, R.P. Singh, E.A. Loria (Ed.), Homogenization and Thermomechanical Processing of Cast Alloy 718, Superalloys 718, 625, 706 and Various Derivatives, The Minerals, Metals & Materials Society, 1991.
- [19] Z. Miao, A. Shan, W. Wang, J. Lu, W. Xu, H. Song, E.A. Ott, et al. (Ed.), Quantitative Characterization of Two-stage Homogenization Treatment of Alloy 718, Superalloys 718 and Derivatives, The Minerals, Metals & Materials Society, 2010.
- [20] C.H. Radhakrishna, K.P. Rao, The formation and control of Laves phase in superalloy 718 welds, J. Mater. Sci. 32 (1997) 1977–1984.
- [21] M.J. Cieslak, T.J. Headley, G.A. Knorovsky, A.D. Romig, T. Kolliea, A comparison of

- the solidification behavior of INCOLOY 909 and INCONEL 718, *Metall. Mater. Trans.* 21 (1990) 479–488.
- [22] W.R. Sun, S.R. Guo, D.Z. Lu, Z.O. Hu, Effect of sulfur on the solidification and segregation in Inconel 718 alloy, *Mater. Lett.* 31 (1997) 195–200.
- [23] K. Chang, H. Lai, J. Hwang, E.A. Loria (Ed.), Existence of Laves Phase in Nb-hardened Superalloys, Superalloys 718,625,706 and Various Derivatives, The Minerals, Metals & Materials Society, 1994.
- [24] S.G. Manikandan, D. Sivakumar, M. Kamaraj, K. Prasad Rao, Laves phase control in Inconel 718 weldments, *Mater. Sci. Forum* 710 (2012) 614–619.
- [25] G. Vander Voort, E.P. Manilova, G.M. Lucas, Metallographic techniques for superalloys, *Microsc. Microanal.* 10 (2004) 690–691.
- [26] G. Petzow, Metallographic Etching, second ed., ASM International, 1999.
- [27] H. Mirzadeh, A simplified approach for developing constitutive equations for modeling and prediction of hot deformation flow stress, *Metall. Mater. Trans.* 46 (2015) 4027–4037.
- [28] M. Naghizadeh, H. Mirzadeh, Microstructural evolutions during annealing of plastically deformed AISI 304 austenitic stainless steel: martensite reversion, grain refinement, recrystallization, and grain growth, *Metall. Mater. Trans.* 47 (2016) 4210–4217.
- [29] H.J. Lucas, A new test for distinguishing the primary, secondary and tertiary saturated alcohols, *J. Am. Chem. Soc.* 52 (1930) 802–804.
- [30] J.F. Radavich, E.A. Loria (Ed.), The Physical Metallurgy of Cast and Wrought alloy 718, Superalloy 718 Metallurgy and Applications, The Minerals, Metals & Materials Society, 1989.
- [31] G.K. Bouse, E.A. Loria (Ed.), Application of a Modified Phase Diagram to the Production of Cast alloy 718 Components, Superalloy 718 Metallurgy and Applications, The Minerals, Metals & Materials Society, 1989.
- [32] W. Ling, G. He, Z. Haofeng, D. Jianxin, Z. Maicang, Phase transformation and liquid density redistribution during solidification of Ni-based superalloy Inconel 718, *China Foundry* 9 (2012) 263–268.
- [33] R.G. Carlson, J.F. Radavich, E.A. Loria (Ed.), Microstructural Characterization of Cast 718, Superalloy 718 Metallurgy and Applications, The Minerals, Metals & Materials Society, 1989.